Available online at www.sciencedirect.com
ScienceDirect
Trans. Nonferrous Met. Soc. China 34(2024) 694−708
Transactions of Nonferrous Metals Society of China
www.tnmsc.cn

Mg recovery from salt lake brine into forsterite refractory materials via precipitation−calcination process

Ye ZHANG[1,2], Yue-hua HU[2], Li WANG[2], Wei SUN[2]

1. National Engineering Research Center for Comprehensive Utilization of Salt Lake Resources, School of Chemical Engineering, East China University of Science and Technology, Shanghai 200237, China;
2. Key Laboratory of Hunan Province for Clean and Efficient Utilization of Strategic Calcium-containing Mineral Resources, School of Minerals Processing and Bioengineering, Central South University, Changsha 410083, China

Received 7 September 2022; accepted 11 April 2023

Abstract: Li/Mg separation and magnesium recovery as a high-value forsterite refractory material from the salt lake were investigated via the precipitation−calcination process. The combined Na_2SiO_3 and NaOH precipitants were applied for Li/Mg precipitation separation from salt lake brine and magnesium precipitates could be produced with various MgO/SiO_2 molar ratios. It is demonstrated that the magnesium precipitates were mainly composed of accumulative amorphous magnesium silicate and magnesium hydroxide, with more than 62% of mass residual at 1400 °C. The high-temperature sintering experiments showed that when the Mg/Na_2SiO_3/NaOH molar ratio was 1:0.6:0.8, the magnesium precipitates could be prepared into a high-quality refractory material under the conditions of 1350 °C and 210 min, with the refractoriness of higher than 1800 °C, compressive strength of 190.73 MPa, bulk density of 2.53 g/cm^3, and apparent porosity of 5.94%. The prepared refractory materials mainly contained forsterite, with a minor enstatite phase.
Key words: salt lake brine; combined precipitants; Li/Mg precipitation separation; magnesium precipitates; forsterite refractory material

1 Introduction

Magnesium is one of the earth's most abundant light metal elements and is known as "the Green Engineering Material in the 21st century" [1−3]. Lithium is considered a strategic energy metal in the 21st century [4]. Lithium and magnesium are abundant in salt lake brine [5]. Several approaches were carried out on Li/Mg separation in salt lake brine, including precipitation [6], adsorption [7], solvent extraction [8], membrane separation [9], and electrochemical methods [10]. Among them, precipitation is a simple and easily-industrialized method. However, many magnesium precipitates are produced as by-products using the magnesium precipitation method [11]. These magnesium by-products would bring great environmental damage without further effective utilization. Therefore, accelerating the green utilization of magnesium by-products is strategically important to sustainable development.

The magnesium precipitation approach was used to investigate various magnesium precipitants during the Li/Mg separation process [11−14]. WANG et al [15] developed a combined precipitant (including $AlCl_3·H_2O$, Na_2CO_3, and NaOH) for recovering magnesium from Taijinar salt lake brine into magnesium−aluminum−carbonate-layered double hydroxide function materials ($MgAlCO_3$−LDHs). These magnesium precipitates could be further treated as valuable materials like catalysts, sorbents,

Corresponding author: Li WANG, Tel: +86-731-88830482, E-mail: li_wang@csu.edu.cn;
Wei SUN, Tel: +86-731-88660477, E-mail: sunmenghu@csu.edu.cn
DOI: 10.1016/S1003-6326(23)66428-3

hosts for nanoscale reactions, and additives to plastic [16−18]. In our previous study [19], a novel magnesium precipitant, sodium metasilicate nonahydrate, was developed for Li/Mg separation in salt lake brine, producing magnesium silicate precipitates during precipitation. From the green recovery process perspective, it is important to utilize these precipitates in a high-value approach.

Generally, several magnesium silicate-based materials have a wide application in the areas of concrete, insulating material, and forsterite refractory materials [20−25]. Among these materials, forsterite refractory materials have a relatively high-value quality and are promising for magnesium silicate-based materials [26]. PAGONA et al [27] investigated the value-added application of magnesite ore mining by-products with 37.5 wt.% SiO_2 and 39.1 wt.% MgO. GU et al [26] used a high-temperature sintering process (1350 °C) to transform a ferronickel slag (48.29 wt.% of silica and 30.95 wt.% of magnesia) into a forsterite refractory material with the addition of sintered magnesia. The prepared refractory material could exhibit refractoriness of 1660 °C and compressive strength of 100.61 MPa. TANG et al [28] developed a microwave irradiation technology with alumina up to 10 wt.% to prepare superior-quality refractory materials with a refractoriness of 1790 °C using ferronickel slag at 1250 °C. Based on the previous research on magnesium silicate-based by-products, the preparation into forsterite refractory materials would be a more appropriate and green treatment approach for magnesium silicate precipitates obtained by Li/Mg precipitation separation from salt lake brine.

Therefore, in this study, Li/Mg precipitation separation process was investigated using various combined precipitants, leading to magnesium precipitates with different SiO_2 and MgO contents. And then, a high-temperature sintering process was applied to these magnesium silicate precipitates to prepare refractory materials. The basic properties of magnesium silicate precipitates were analyzed. Relevant parameters and mechanisms during the sintering process were studied in detail.

2 Experimental

2.1 Materials

$LiCl·H_2O$ (AR, 97.0%, Sinopharma Chemical Reagent Co., Ltd., China) and $MgCl_2·6H_2O$ (AR, 99.0%, Sinopharma Chemical Reagent Co., Ltd., China) were used to prepare simulated salt lake brine (2 g/L Li^+ and 60 g/L Mg^{2+}). Sodium metasilicate (AR, SiO_2 44−47 wt.%, Shanghai Macklin Biochemical Co., Ltd., China) and sodium hydroxide (AR, 96.0%, Sinopharma Chemical Reagent Co., Ltd., China) were used to precipitate Mg^{2+} in simulated salt lake brine.

2.2 Methods

2.2.1 Precipitation experiments

The precipitation experiments were carried out on an electric blender (OES−20M, Changzhou Zhengrong Instrument Co., Ltd., China). A certain amount of Na_2SiO_3 and NaOH were dissolved in the solution and added drop by drop into simulated salt lake brine to precipitate Mg^{2+}. The precipitation conditions were set as a reaction time of 5 min and an agitation rate of 600 r/min. The precipitant dosages (molar ratio) were set as n(Mg): n(Na_2SiO_3):n(NaOH) of 1:1:0, 1:0.8:0.4, 1:0.6:0.8, 1:0.4:1.2, and 1:0.2:1.6, respectively. Magnesium precipitates with various MgO/SiO_2 molar ratios can be obtained after precipitation experiments.

2.2.2 Sintering experiments

Firstly, magnesium precipitates obtained from precipitation experiments were ground below 75 μm using a three-head grinder (XPM-d120 mm×3, Nanchang Jianfeng Mining Machinery Equipment Co., Ltd., China). And then, the fine magnesium precipitates and deionized water (10 wt.%) were mixed. The mixtures were pressed into flaky samples using a hydraulic press (Changshu Tongrun Auto Parts Co., Ltd., China). Finally, the flaky samples were put into a tubular high-temperature furnace (GSL−1700X, Hefei Kejing Material Technology Co., Ltd., China) for sintering experiments under specific conditions and refractory materials.

2.2.3 Characterization

Crystalline structure and phase compositions of magnesium precipitates and refractory materials were analyzed using an X-ray diffractometer (Advance D8, BRUKER, Switzerland). The particle size distribution of magnesium precipitate was analyzed using a laser particle size analyzer (Mastersizer 2000, Malvern, England). The surface morphology and element composition of magnesium precipitates and refractory materials

were analyzed using a scanning electron microscope with energy dispersive X-ray spectroscopy (SEM−EDS) (JSM−7001F, JEOL, Japan). The mass change and heat change during the sintering process of magnesium precipitates were analyzed using a synchronous thermal analyzer (NETZSCH STA 2500, NETZSCH, Germany). The compressive strength of refractory materials was measured according to the Chinese National Standard Test Method (GBT 5072—2008). The bulk density and apparent porosity of refractory materials were measured according to the Chinese National Standard Test Method (GBT 2997—2000). The refractoriness of refractory materials was measured by complying with the Chinese National Standard Test Method (GBT 7322—2017).

3 Results and discussion

3.1 Li/Mg precipitation separation

Our previous study [13] demonstrated that sodium silicate could be used as an efficient magnesium precipitant during the Li/Mg separation process. Meanwhile, a large amount of amorphous magnesium silicate precipitates were produced, whose composition mainly contained magnesia and silica. These precipitates can be used to produce the forsterite refractory materials for their value-added and bulk utilization. As reported, pure forsterite has a MgO/SiO_2 molar ratio of approximately 2.0 [29]. However, the magnesium silicate precipitates obtained only using sodium silicate have a low MgO/SiO_2 molar ratio of 1.08, which may not be suitable for preparing high-performance forsterite refractory materials. Given this problem, combined sodium silicate and sodium hydroxide precipitants were developed for precipitating magnesium ions and producing magnesium precipitates with high MgO/SiO_2 molar ratios.

Combined precipitants with five kinds of n(Mg):n(Na_2SiO_3):n(NaOH) were used for Li^+/Mg^{2+} precipitation separation and producing precipitates with various MgO/SiO_2 molar ratios. The results of the precipitation process are shown in Fig. 1. As shown in the figure, during the whole range of n(Mg):n(Na_2SiO_3):n(NaOH), the Mg recovery and Li recovery in precipitates were kept constant at >98% and <6%, respectively, indicating that Mg^{2+} was precipitated efficiently, with Li^+ left in the solution. Mg^{2+} and Li^+ could be effectively separated from salt lake brine. The magnesium precipitates probably comprised magnesium silicate and magnesium hydroxide, which showed a negatively charged surface during the precipitation system [30,31]. Thus, Li^+ may be adsorbed and entrained on the surface of magnesium precipitates, causing a small Li^+ loss in magnesium precipitates.

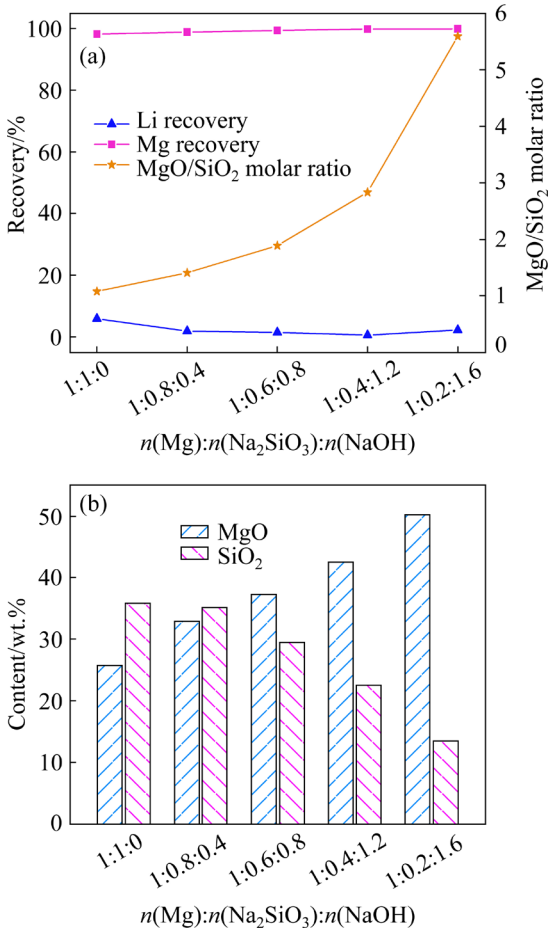

Fig. 1 Variation of Li and Mg recoveries and MgO/SiO_2 molar ratio (a), and MgO and SiO_2 contents (b) in precipitates as function of n(Mg):n(Na_2SiO_3):n(NaOH)

In addition, with the increase in NaOH proportion of n(Mg):n(Na_2SiO_3):n(NaOH), the MgO content in precipitates increased gradually from 25.8 wt.% to 50.3 wt.%, meanwhile, the SiO_2 content in precipitates decreased steadily from 35.89 wt.% to 13.5 wt.%, leading to the MgO/SiO_2 molar ratio in precipitates increasing progressively from 1.08 to 5.60 correspondingly. This is because the increased NaOH proportion in the combined precipitant could produce a high amount of $Mg(OH)_2$ in magnesium precipitates and bring a high MgO content. Therefore, as can be concluded, the combined sodium silicate and NaOH

precipitants can not only achieve effective Li^+/Mg^{2+} separation but also improve the MgO/SiO_2 molar ratio of magnesium precipitates for further refractory materials preparation.

3.2 Properties of magnesium precipitates

3.2.1 Phase composition

During the precipitation process, Li^+ and Mg^{2+} in salt lake brine can react with SiO_3^{2-} and OH^- according to Reactions (1)−(4) when the combined sodium silicate and NaOH precipitants were added. It is demonstrated that $Mg(OH)_2$ and $MgSiO_3$ are lower solubility products at 25 °C [32,33]. In contrast, LiOH and Li_2SiO_3 are soluble in the brine. Therefore, Mg^{2+} can be precipitated as $Mg(OH)_2$ and $MgSiO_3$, with Li^+ in the solution.

$$Li^+(aq)+OH^-(aq)=LiOH(aq) \quad (1)$$

$$2Li^+(aq)+SiO_3^{2-}(aq)=Li_2SiO_3(aq) \quad (2)$$

$$Mg^{2+}(aq)+2OH^-(aq)=Mg(OH)_2(s) \quad (3)$$

$$nMg^{2+}(aq)+SiO_3^{2-}(aq)=Mg_nSiO_3(s) \quad (4)$$

The phase composition and crystalline structure of magnesium precipitates were analyzed using X-ray diffraction. The results are shown in Fig. 2. As shown in the figure, when the n(Mg):n(Na_2SiO_3):n(NaOH) were 1:1:0, 1:0.8:0.4, and 1:0.6:0.8, the magnesium precipitates were mainly composed of amorphous magnesium silicates. When the n(Mg):n(Na_2SiO_3):n(NaOH) was 1:0.4:1.2, the characteristic peaks of brucite appeared at 2θ values of 18.527° and 37.983°, besides characteristic peaks of the magnesium silicate. When the n(Mg):n(Na_2SiO_3):n(NaOH) was 1:0.2:1.6, the magnesium precipitates were mainly composed of brucite and minor magnesium silicate. The XRD results indicate that the increased NaOH proportion in combined precipitants could increase the brucite content in magnesium precipitates. Therefore, the increased NaOH content in combined precipitants could increase the MgO content in magnesium precipitates. Moreover, the XRD results were consistent with the element composition results of magnesium precipitates.

3.2.2 Particle size distribution

The particle size distribution and cumulative distribution of various magnesium precipitates are shown in Fig. 3. The D_{10}, D_{50}, D_{90}, and average particle sizes of various magnesium precipitates are shown in Table 1. As shown in Fig. 3 and Table 1, all five magnesium precipitates showed a normal particle size distribution, indicating that the magnesium precipitates had a uniform and concentrated particle size distribution. With the increase of NaOH proportion in combined precipitant, the average particle size of magnesium precipitates decreased from 27.492 to 17.942 μm, and the particle size distribution was more concentrated, probably because the average particle

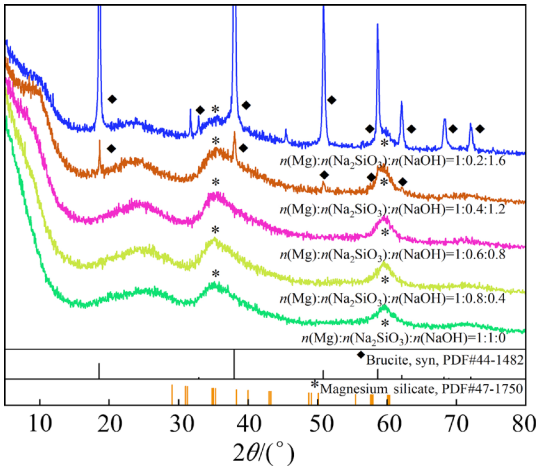

Fig. 2 XRD patterns of various magnesium precipitates

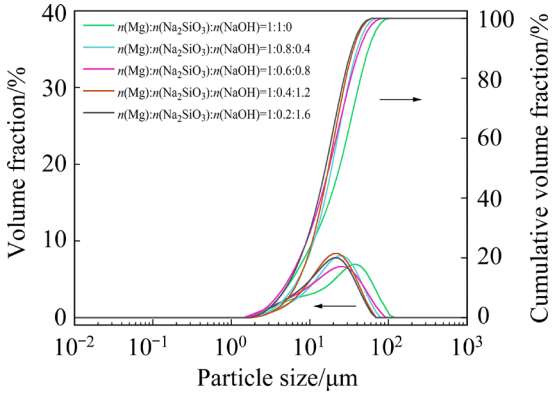

Fig. 3 Particle size distribution and cumulative distribution of various magnesium precipitates

Table 1 D_{10}, D_{50}, D_{90}, and average particle size of various magnesium precipitates

n(Mg): n(Na_2SiO_3): n(NaOH)	D_{10}/ μm	D_{50}/ μm	D_{90}/ μm	Average particle size/μm
1:1:0	5.023	23.691	56.018	27.492
1:0.8:0.4	6.086	18.903	40.174	21.346
1:0.6:0.8	4.6	17.464	43.105	21.096
1:0.4:1.2	6.412	17.219	35.893	19.459
1:0.2:1.6	4.933	15.743	34.223	17.942

size of the obtained brucite was lower than that of the obtained magnesium silicate. The increased NaOH proportion in combined precipitant was contributed to a high brucite content in magnesium precipitates, which resulted in the decreased average particle size of magnesium precipitates.

3.2.3 Thermal stability

The dehydration property and thermal stability of magnesium precipitates were analyzed using TG−DSC, and the results are shown in Fig. 4. As shown in Figs. 4(a) and (b), the mass of magnesium precipitates suffered from a rapid decrease at 100−110 °C and 350−400 °C. When the temperature was higher than 400 °C, the mass of magnesium precipitates dropped slowly and then declined rapidly at 700−800 °C. The residual mass fractions of five kinds of magnesium precipitates were 68.05%, 66.70%, 64.51%, 62.75%, and 62.66% at 1400 °C, when the n(Mg): n(Na_2SiO_3): n(NaOH) was 1:1:0, 1:0.8:0.4, 1:0.6:0.8, 1:0.4:1.2, and 1:0.2:1.6, respectively (Fig. 4(a)). As shown in Fig. 4(c), all magnesium precipitates have two endothermic peaks and one exothermic peak. The endothermic peak at approximately 110 °C was probably attributed to the dehydration reaction of free water in precipitates. The endothermic peak at 350−400 °C may be due to the decomposition of magnesium hydroxide and the intensity of peaks increased with the increase of the NaOH proportion in combined precipitant. The exothermic peak at 700−800 °C may be derived from the phase transformation and the intensity of peaks increased with the increase of the Na_2SiO_3 proportion in combined precipitant. The DSC analysis results were also consistent with the TG analysis results.

3.2.4 Surface morphology and element composition

The surface morphology and element composition of magnesium precipitates were analyzed using SEM−EDS analysis. The results are shown in Fig. 5. As shown in the figure, when the n(Mg):n(Na_2SiO_3):n(NaOH) was 1:1:0, 1:0.8:0.4, 1:0.6:0.8, and 1:0.4:1.2, the surfaces of the prepared refractory materials were dense. When the n(Mg): n(Na_2SiO_3):n(NaOH) was 1:0.2:1.6, the surface of the prepared refractory materials was relatively loose. The particles showed mainly irregular shapes and structures, and the magnesium precipitates comprised accumulative amorphous particles. The size of particles gradually decreased and the particle

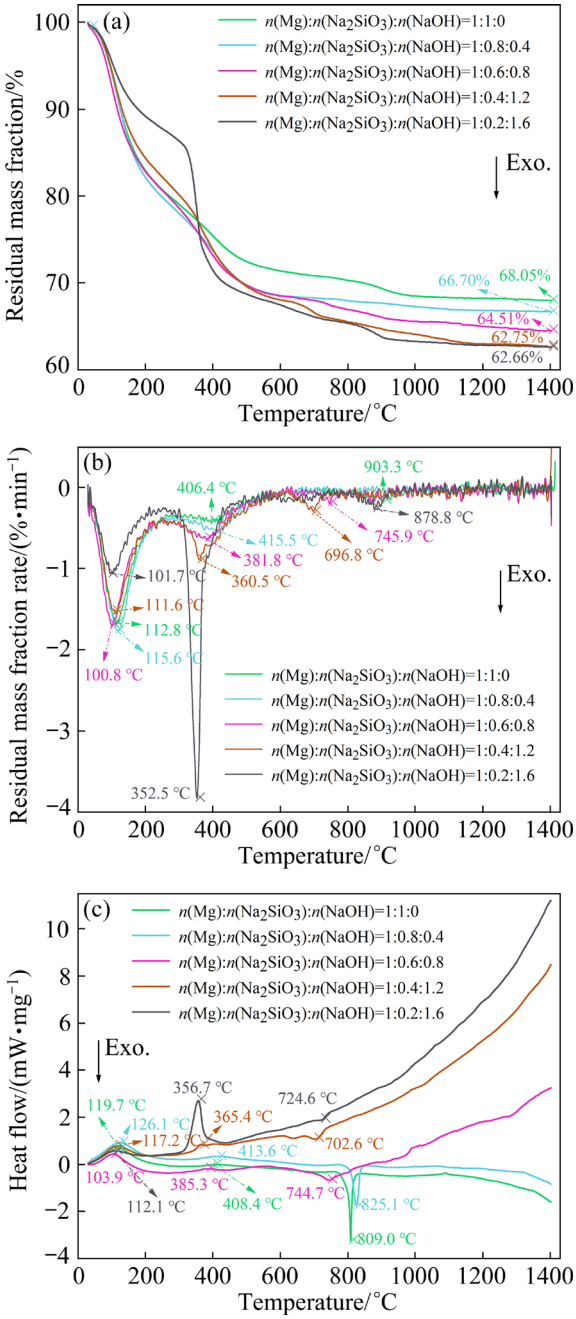

Fig. 4 TG (a), DTG (b), and DSC (c) curves of various magnesium precipitates

accumulation became closer and closer, with the increased NaOH proportion in combined precipitant. This is probably owing to the high brucite content in magnesium precipitates caused by increased NaOH proportion in combined precipitant. Therefore, the solid-state reaction may be easier during further sintering experiments [34−36]. EDS results showed that the Mg content of magnesium precipitates increased with the increase of the NaOH proportion in the combined precipitant. This can match the results of precipitation experiments.

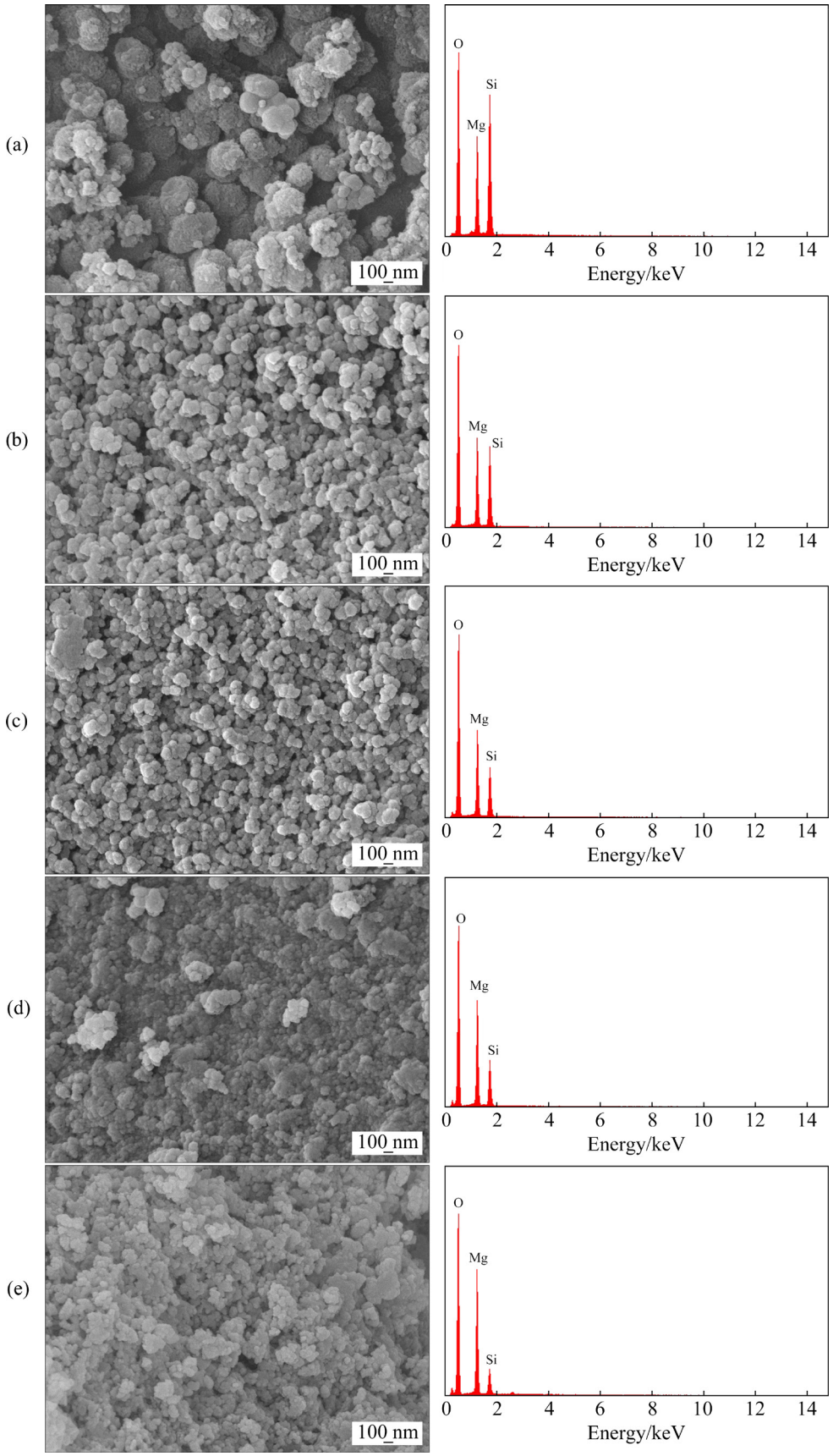

Fig. 5 SEM−EDS analysis results of magnesium precipitates obtained at different n(Mg):n(Na_2SiO_3):n(NaOH): (a) 1:1:0; (b) 1:0.8:0.4; (c) 1:0.6:0.8; (d) 1:0.4:1.2; (e) 1:0.2:1.6

3.3 Preparation of refractory materials

Five kinds of magnesium precipitates with MgO/SiO_2 molar ratios ranging from 1.08 to 5.60 were obtained during the precipitation process by using combined precipitants and used for preparing forsterite refractory materials. The influences of sintering temperature and sintering time on the preparation of forsterite refractory materials were investigated, and the properties of five kinds of forsterite refractory materials were determined and compared.

3.3.1 Sintering temperature

The influence of sintering temperature on the properties of refractory materials obtained using various magnesium precipitates is shown in Fig. 6. As shown in Fig. 6(a), when the n(Mg):n(Na_2SiO_3):n(NaOH) was 1:1:0, 1:0.8:0.4, and 1:0.6:0.8, the compressive strength of refractory materials increased with the increase of sintering temperature and peaked at 1350 °C. When the n(Mg):n(Na_2SiO_3):n(NaOH) was 1:0.4:1.2 and 1:0.2:1.6, the compressive strength of refractory materials increased with increasing the sintering temperature. It was lower than that of the refractory materials obtained at n(Mg):n(Na_2SiO_3):n(NaOH) of 1:1:0, 1:0.8:0.4, and 1:0.6:0.8 when the temperature was less than 1350 °C. This may be due to a large amount of magnesium hydroxide in magnesium precipitates. As shown in Fig. 6(b), when the n(Mg):n(Na_2SiO_3):n(NaOH) was 1:1:0, 1:0.8:0.4, and 1:0.6:0.8, the bulk density of refractory materials remained at 2.2−2.6 g/cm^3 during the whole range of sintering temperature and was higher than that of refractory materials obtained at n(Mg):n(Na_2SiO_3):n(NaOH) of 1:0.4:1.2 and 1:0.2:1.6. As shown in Fig. 6(c), when the n(Mg):n(Na_2SiO_3):n(NaOH) was 1:1:0, 1:0.8:0.4, and 1:0.6:0.8, the apparent porosity of refractory materials kept constant at 15%, 11%, and 8%, respectively, during the whole range of sintering temperature. When the n(Mg):n(Na_2SiO_3):n(NaOH) was 1:0.4:1.2 and 1:0.2:1.6, the apparent porosity of refractory materials decreased with increasing the sintering temperature and remained at above 30%. Therefore, 1350 °C was selected as the optimal sintering temperature, at which refractory materials had higher compressive strength, bulk density, and lower apparent porosity.

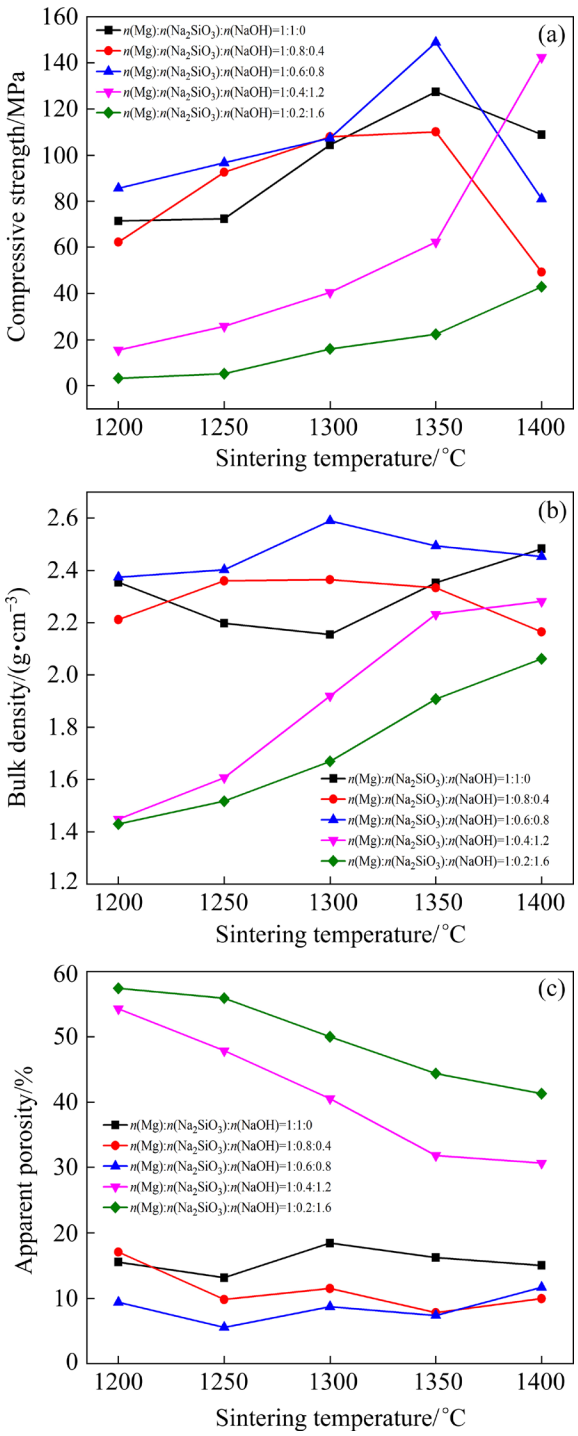

Fig. 6 Compressive strength (a), bulk density (b), and apparent porosity (c) of refractory materials obtained using various magnesium precipitates at various sintering temperatures

3.3.2 Sintering time

The influence of the sintering time on the properties of refractory materials obtained using various magnesium precipitates is shown in Fig. 7. As shown in Fig. 7(a), when the n(Mg):n(Na_2SiO_3):n(NaOH) was 1:1:0, the compressive strength of the refractory materials increased from 90.98 to

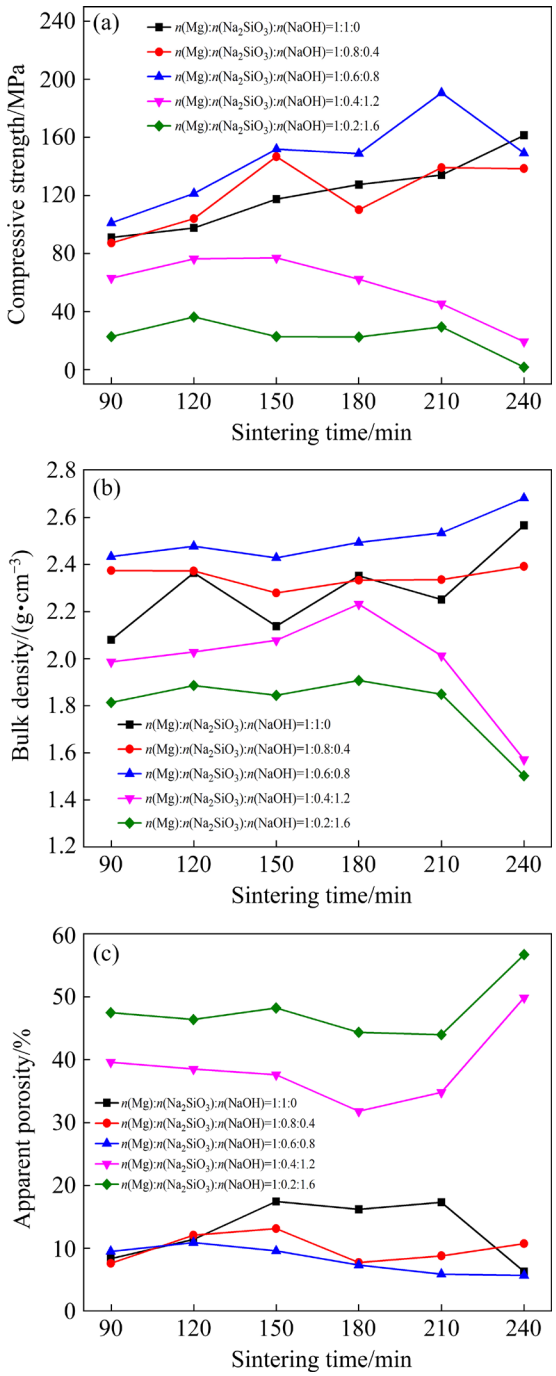

Fig. 7 Compressive strength (a), bulk density (b), and apparent porosity (c) of refractory materials obtained using various magnesium precipitates at various sintering time

161.45 MPa with increasing sintering time from 90 to 240 min. When the n(Mg):n(Na_2SiO_3):n(NaOH) was 1:0.8:0.4, the compressive strength of refractory materials peaked at 146.72 MPa, at the sintering time of 150 min, and then basically remained stable. When the n(Mg):n(Na_2SiO_3):n(NaOH) was 1:0.6:0.8, the compressive strength of refractory materials increased with increasing the sintering time and peaked at the sintering time of 210 min. When the n(Mg):n(Na_2SiO_3):n(NaOH) was 1:0.4:1.2 and 1:0.2:1.6, the compressive strength of refractory materials remained below 80 MPa and 20−30 MPa, respectively, during the whole range of sintering time. As shown in Fig. 7(b), when the n(Mg):n(Na_2SiO_3):n(NaOH) was 1:1:0, 1:0.8:0.4, and 1:0.6:0.8, the bulk density of refractory materials increased slightly with increasing the sintering time, remaining above 2.1 g/cm^3 and higher than that of refractory materials obtained at n(Mg):n(Na_2SiO_3):n(NaOH) of 1:0.4:1.2 and 1:0.2:1.6. As shown in Fig. 7(c), when the n(Mg):n(Na_2SiO_3):n(NaOH) was 1:1:0, 1:0.8:0.4, and 1:0.6:0.8, the apparent porosity of refractory materials kept constant below 15% during the whole range of sintering temperature. When n(Mg):n(Na_2SiO_3):n(NaOH) was 1:0.4:1.2 and 1:0.2:1.6, the apparent porosity of refractory materials decreased with increasing the sintering temperature at sintering time less than 210 min and remained at above 30% and 40%, respectively. Therefore, 210 min was selected as the optimal sintering time, where the refractory materials had higher compressive strength, bulk density, and lower apparent porosity.

3.4 Properties of refractory materials

The physical drawing of refractory materials obtained under the optimum condition is shown in Fig. 8. The compressive strength, bulk density, apparent porosity, and refractoriness of refractory materials obtained under the optimum condition are shown in Fig. 9. As shown in Fig. 9(a), with the increase of NaOH proportion in combined precipitant, the compressive strength of refractory materials increased gradually from 134.13 to 190.73 MPa. It then decreased rapidly to 29.37 MPa, peaking at n(Mg):n(Na_2SiO_3):n(NaOH) of 1:0.6:0.8. Figure 9(b) showed that the changing trend of bulk density of refractory materials was similar to compressive strength. The bulk density of refractory materials peaked at 2.53 g/cm^3 at n(Mg):n(Na_2SiO_3):n(NaOH) of 1:0.6:0.8. It was shown in Fig. 9(c) that the changing trend of apparent porosity of refractory materials was opposite to that of compressive strength and bulk density. The apparent porosity of refractory materials dropped gradually from 17.35% to 5.94%. It then increased sharply to 44.01%, reaching the

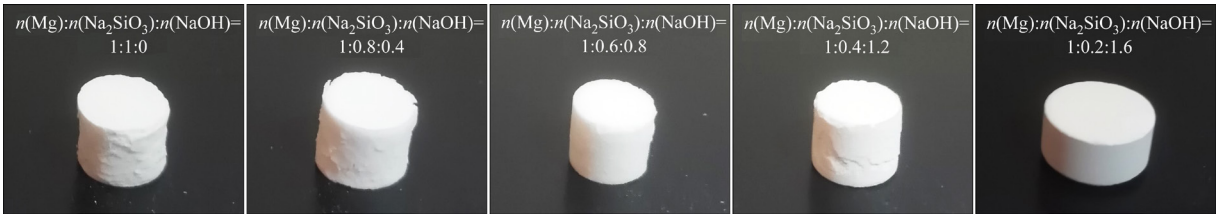

Fig. 8 Physical drawing of refractory materials obtained under optimum condition

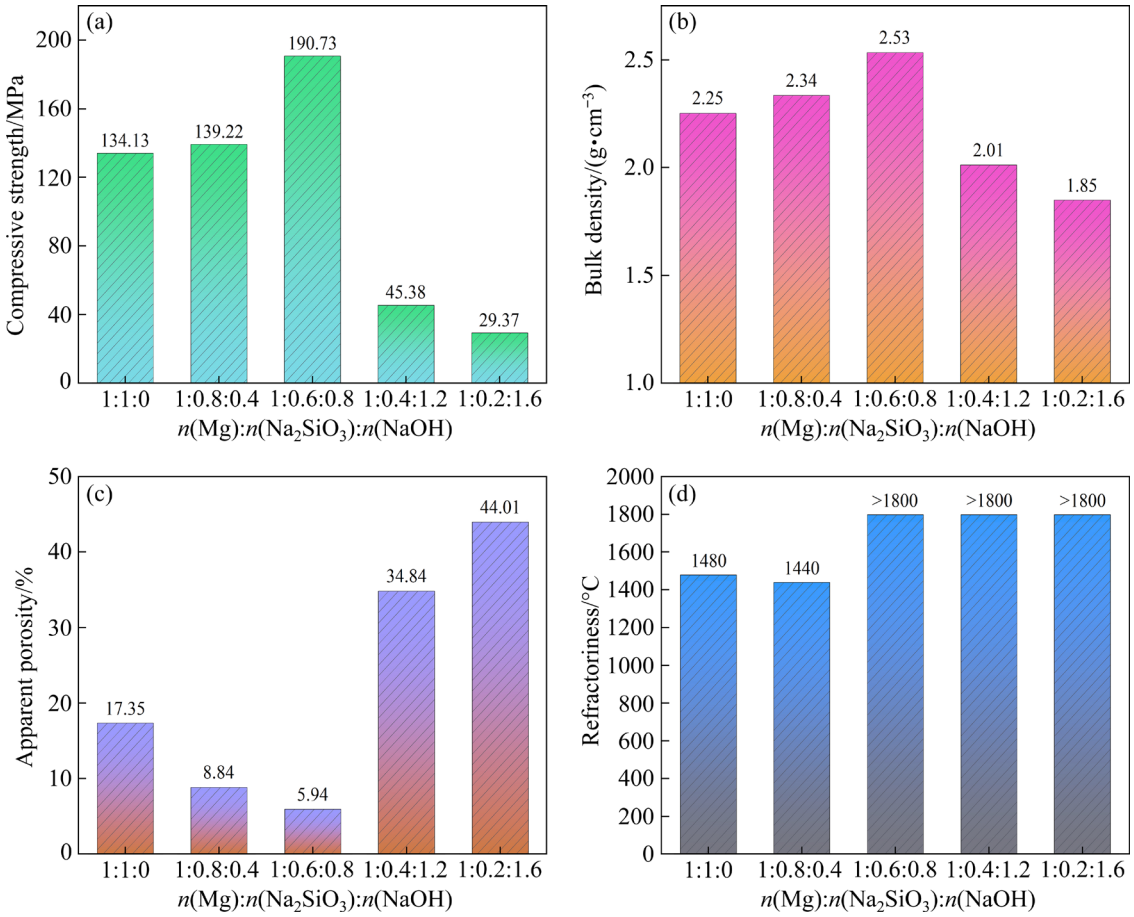

Fig. 9 Compressive strength (a), bulk density (b), apparent porosity (c), and refractoriness (d) of refractory materials obtained under optimum sintering condition

minimum at the n(Mg):n(Na_2SiO_3):n(NaOH) of 1:0.6:0.8. As shown in Fig. 9(d), when the n(Mg):n(Na_2SiO_3):n(NaOH) was 1:1:0 and 1:0.8:0.4, the refractoriness of refractory materials was similar, at 1480 and 1440 °C, respectively. When the n(Mg):n(Na_2SiO_3):n(NaOH) was 1:0.6:0.8, 1:0.4:1.2, and 1:0.2:1.6, the refractoriness of refractory materials reached more than 1800 °C. In conclusion, when the n(Mg):n(Na_2SiO_3):n(NaOH) was 1:0.6:0.8, the magnesium precipitates could be prepared into a high-quality refractory material under the optimum sintering condition of 1350 °C and 210 min, with the refractoriness of higher than 1800 °C, compressive strength of 190.73 MPa, bulk density of 2.53 g/cm^3, and apparent porosity of 5.94%.

3.5 Thermodynamic analysis results and phase transformation mechanism

3.5.1 Thermodynamic analysis results

Figure 10 shows the calculated contents of thermodynamic equilibrium phases of various magnesium precipitates in the temperature range of 800−1600 °C. As can be seen, when the n(Mg):n(Na_2SiO_3):n(NaOH) was 1:1:0, 1:0.8:0.4, and 1:0.6:0.8, the main equilibrium phases of prepared magnesium precipitates at high temperatures are

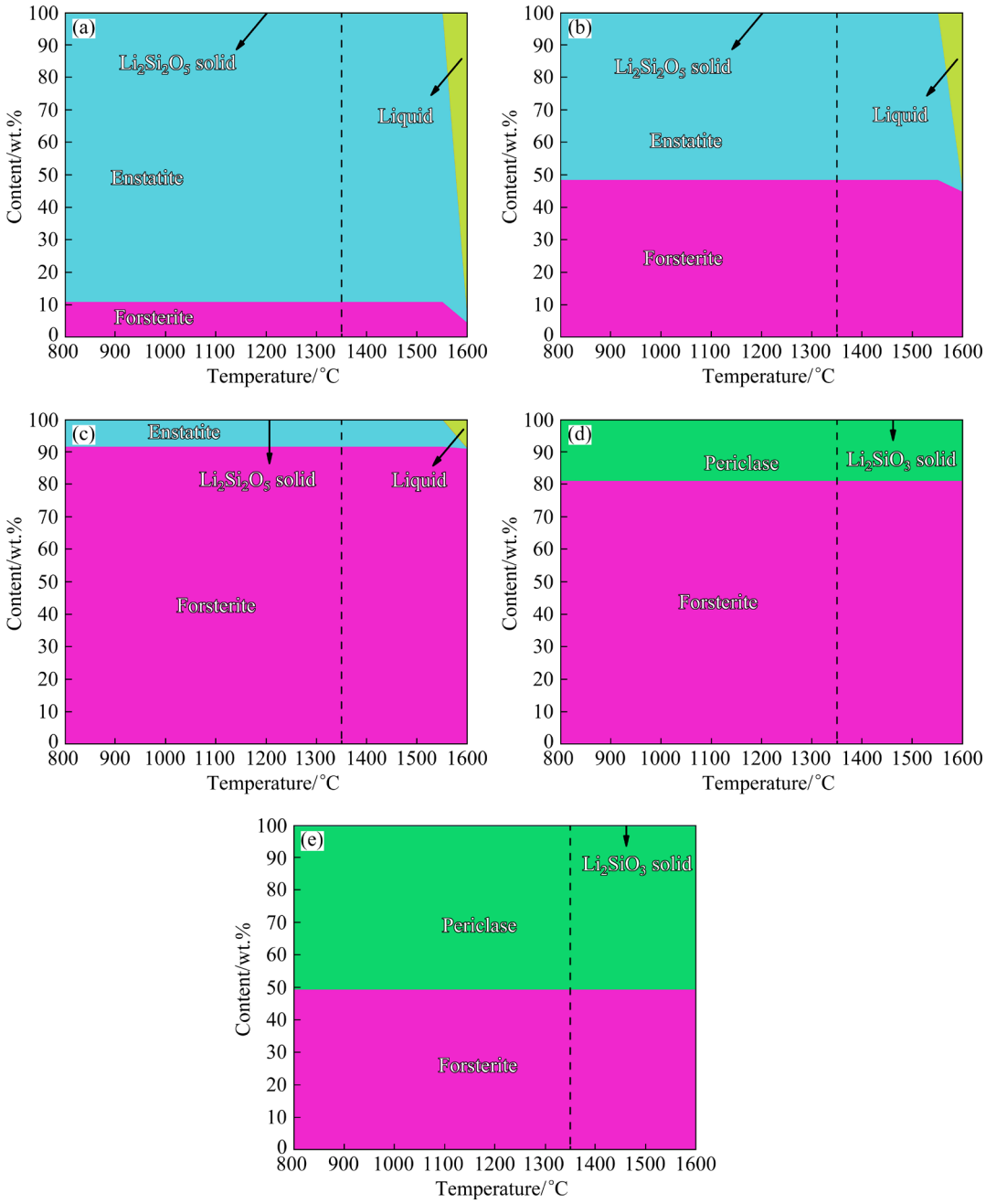

Fig. 10 Calculated contents of thermodynamic equilibrium phases of various magnesium precipitates at 800−1600 °C and different n(Mg):n(Na_2SiO_3):n(NaOH): (a) 1:1:0; (b) 1:0.8:0.4; (c) 1:0.6:0.8; (d) 1:0.4:1.2; (e) 1:0.2:1.6

forsterite (melting point: 1890 °C) and enstatite (melting point: 1543 °C). The formation of these phases is probably attributed to the decomposition and oxidation of olivine in the air atmosphere [26]. The liquid phase appeared when the temperature exceeded 1550 °C. With the increase of NaOH proportion in combined precipitants, contents of the enstatite and liquid phases gradually decreased, but the forsterite content increased. When the n(Mg):n(Na_2SiO_3):n(NaOH) was 1:0.4:1.2 and 1:0.2:1.6, the main equilibrium phases of prepared magnesium precipitates at high temperatures were periclase and forsterite. These two phases may be due to the thermal decomposition of brucite and the oxidation of olivine in the air atmosphere [26,37]. With the increase of NaOH proportion in combined precipitants, the content of the forsterite phase declined while that of the periclase phase increased.

Overall, with the increase of NaOH proportion in combined precipitants, the enstatite content in the equilibrium phase declined while the periclase phase increased. The content of the forsterite phase

increased firstly and then suffered from a decline, reaching a peak when the n(Mg):n(Na_2SiO_3):n(NaOH) in combined precipitant was 1:0.6:0.8. Therefore, it can be seen that the appropriate NaOH proportion in the combined precipitant could facilitate the formation of forsterite and depress the formation of enstatite, periclase, and liquid phase during the sintering process.

3.5.2 X-ray diffraction analysis results

The five magnesium precipitates obtained during precipitation mainly contained amorphous magnesium silicate and brucite. Therefore, the magnesium precipitates would undergo Reactions (5)−(8) during the sintering process. The brucite will be decomposed into periclase when the temperature rises to 400 °C [38,39]. With the increase in temperature, the structural water will release from the precipitates (dehydroxylation stage), and the magnesium silicate will be formed at 700−800 °C, as shown in Reaction (6) [40−42]. The formed magnesium silicate will change into forsterite (Mg_2SiO_4). Free silica (SiO_2) will be produced at 835 °C, followed by the reaction of forsterite with free silica at 1000−1150 °C to form forsterite and enstatite ($MgSiO_3$) [40,42−44]. Besides, the enstatite phase can change into protoenstatite [44]. The increased brucite content in magnesium precipitates can promote the transformation of the origin phase from magnesium silicate into forsterite.

$$Mg(OH)_2(s)=MgO(s)+H_2O(g) \quad (5)$$

$$Mg_3(Si_2O_5)(OH)_4(s)=3MgO\cdot 2SiO_2(s)+2H_2O(g) \quad (6)$$

$$2(3MgO\cdot 2SiO_2)(s)=3Mg_2SiO_4(s)+SiO_2(s) \quad (7)$$

$$3Mg_2SiO_4(s)+SiO_2(s)=2Mg_2SiO_4(s)+2MgSiO_3(s) \quad (8)$$

The crystalline structure and phase composition of refractory materials are shown in Fig. 11. When the n(Mg):n(Na_2SiO_3):n(NaOH) was 1:1:0, the prepared refractory materials mainly contained forsterite and protoenstatite, with a tiny amount of clinoenstatite. When the n(Mg):n(Na_2SiO_3):n(NaOH) was 1:0.8:0.4, the prepared refractory materials mainly contained forsterite, with minor protoenstatite. When the n(Mg):n(Na_2SiO_3):n(NaOH) was 1:0.6:0.8, the prepared refractory materials were mainly composed of forsterite. When the n(Mg):n(Na_2SiO_3):n(NaOH) was 1:0.4:1.2, the prepared refractory materials contained forsterite and minor periclase. When the n(Mg):n(Na_2SiO_3):n(NaOH) was 1:0.2:1.6, the prepared refractory materials were mainly composed of forsterite and periclase. As shown in Fig. 11(b), all five refractory materials contained forsterite. With the increase of NaOH proportion in combined precipitant, the content of the forsterite phase in refractory materials increased firstly, peaking at n(Mg):n(Na_2SiO_3):n(NaOH) of 1:0.6:0.8, and then decreased. The enstatite and amorphous phases only appeared by using magnesium precipitates obtained at a lower NaOH proportion in the combined precipitant. In comparison, the periclase phase only appeared by using magnesium precipitates obtained at the higher NaOH proportion in the combined precipitant.

3.5.3 SEM−EDS analysis results

The surface morphology and element composition of five kinds of refractory materials are shown in Fig. 12. As shown, all five kinds of refractory materials consisted of well-crystalline

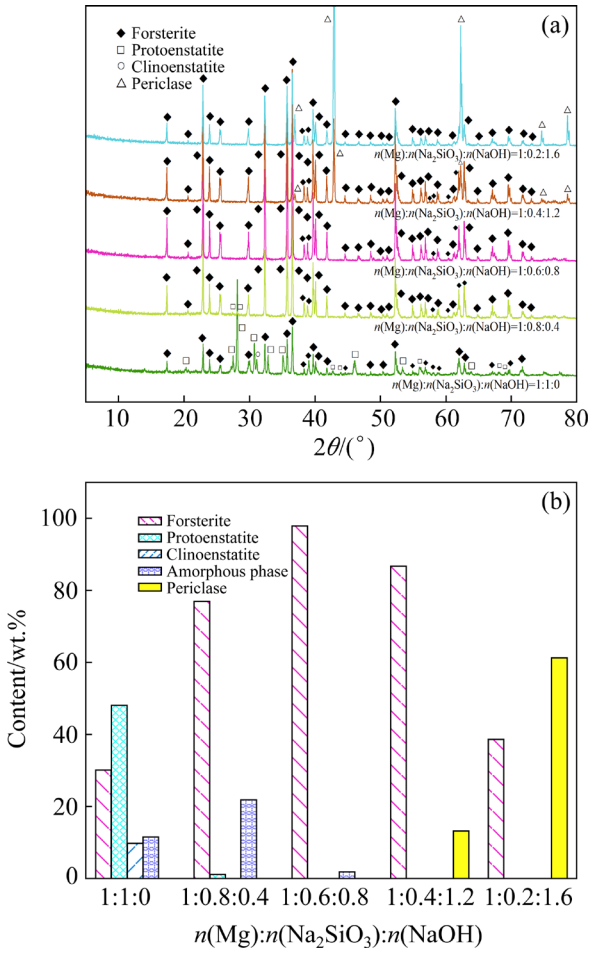

Fig. 11 XRD patterns (a) and contents of phases (b) of refractory materials prepared under optimum sintering condition

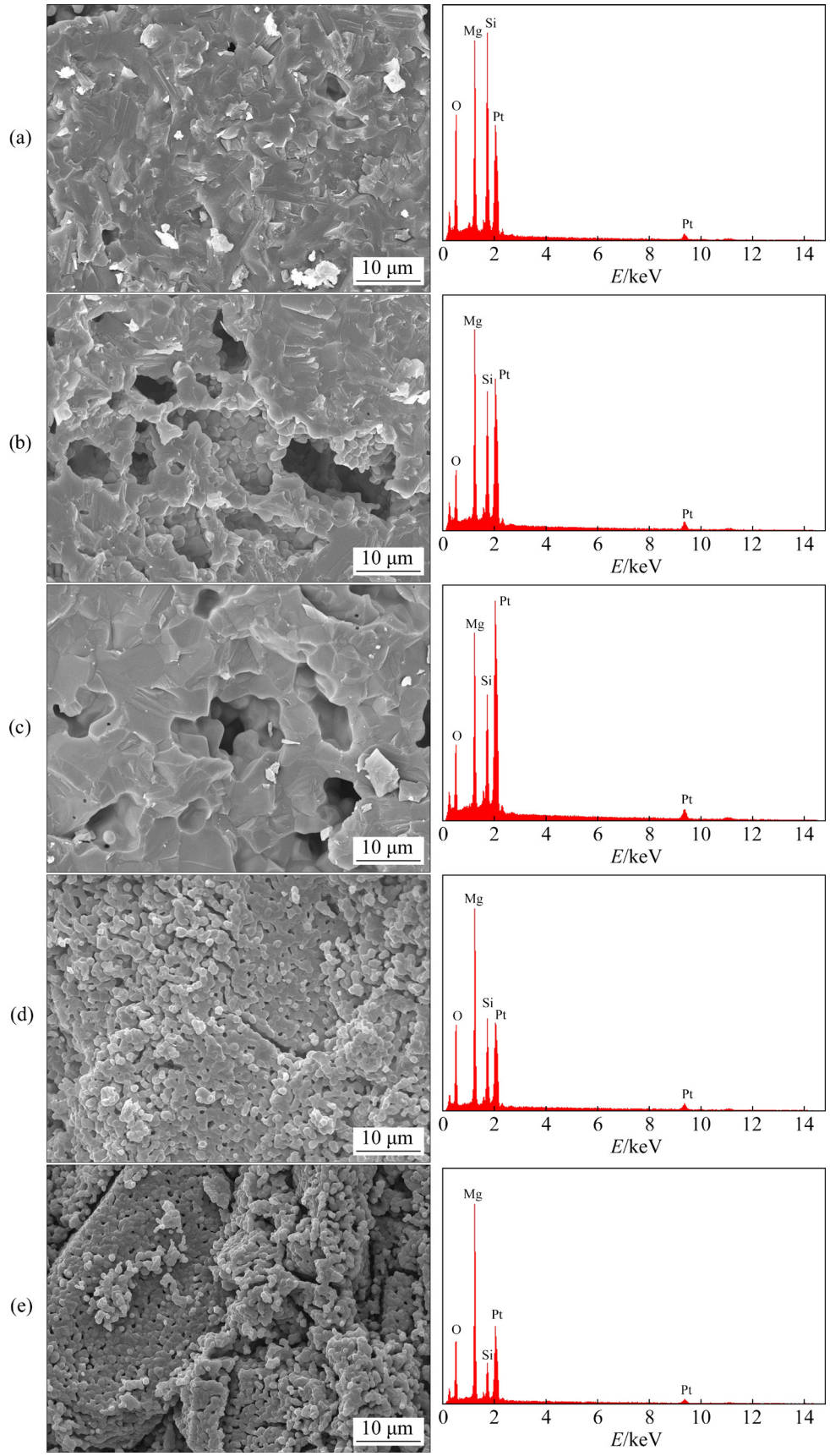

Fig. 12 SEM−EDS analysis results of refractory materials prepared from magnesium precipitates obtained at different n(Mg):n(Na_2SiO_3):n(NaOH): (a) 1:1:0; (b) 1:0.8:0.4; (c) 1:0.6:0.8; (d) 1:0.4:1.2; (e) 1:0.2:1.6

grains. When the n(Mg):n(Na_2SiO_3): n(NaOH) was 1:1:0, 1:0.8:0.4, and 1:0.6:0.8, there were many densely connected pores in the surface of prepared refractory materials. With the increased NaOH proportion in combined precipitant, the grain size became larger, and the pore size became smaller. This may be contributed to the increased content of the well-crystalline forsterite phase in prepared refractory materials. When the n(Mg):n(Na_2SiO_3): n(NaOH) was 1:0.4:1.2 and 1:0.2:1.6, the surfaces of refractory materials were very loose, and the grain size was smaller than that of the other three refractory materials. This may be attributed to the increased content of the periclase phase in prepared refractory materials. EDS results showed that with the increased NaOH proportion in combined precipitant, the magnesium content in refractory materials increased, and the silicon content in refractory materials decreased.

4 Conclusions

(1) The combined Na_2SiO_3 and NaOH precipitants were used for Mg^{2+} precipitation during the Li/Mg separation process in salt lake brine. Effective Li^+/Mg^{2+} precipitation separation could be achieved and magnesium precipitates with various MgO/SiO_2 molar ratios could be obtained.

(2) The MgO/SiO_2 molar ratio in magnesium precipitates increased from 1.08 to 5.60 with the increased NaOH proportion in combined precipitants. The magnesium precipitates mainly contained amorphous magnesium silicate and brucite and had a uniform particle size distribution. They had more than 62% of residual mass fraction at 1400 °C, with two endothermic peaks at approximately 110 °C and 350−400 °C, respectively, and one exothermic peak at 700−800 °C.

(3) The thermodynamic analysis showed that the magnesium precipitates obtained under an appropriate n(Mg):n(Na_2SiO_3):n(NaOH) could be transformed into sintering products with a high forsterite content in the temperature range from 800 to 1600 °C. The amorphous magnesium silicate phase in magnesium precipitates could be transformed into a forsterite phase in the temperature range of 800−1600 °C.

(4) When the n(Mg):n(Na_2SiO_3):n(NaOH) was 1:0.6:0.8, the magnesium precipitates could be prepared into a high-quality refractory material under the sintering conditions of 1350 °C and 210 min, with the refractoriness of higher than 1800 °C, compressive strength of 190.73 MPa, bulk density of 2.53 g/cm^3, and apparent porosity of 5.94%.

CRediT authorship contribution statement

Ye ZHANG: Conceptualization, Methodology, Writing − Original draft, Writing − Review & editing, Project administration, Funding acquisition; **Yue-hua HU:** Methodology, Resources, Supervision; **Li WANG:** Conceptualization, Methodology, Formal analysis, Visualization, Funding acquisition; **Wei SUN:** Conceptualization, Resources, Supervision, Funding acquisition.

Declaration of competing interest

The authors declare that they have no known competing financial interests or personal relationships that could have appeared to influence the work reported in this paper.

Acknowledgments

We gratefully appreciate the financial supports from the National Natural Science Foundation of China (Nos. 52204268, 51974365, 91962223), the Natural Science Foundation of Hunan Province, China (Nos. 2020JJ5747, 2020JJ5749), the Innovation-driven Project of Central South University, China (No. 2020CX039), the National “111” Project of China (No. B14034), the Key Laboratory of Hunan Province for Clean and Efficient Utilization of Strategic Calcium-containing Mineral Resources, China (No. 2018TP1002), and the Young Elite Scientists Sponsorship Program by CAST, China (No. 2019QNRC001).

References

[1] XU Tian-cai, YANG Yan, PENG Xiao-dong, SONG Jiang-feng, PAN Fu-sheng. Overview of advancement and development trend on magnesium alloy [J]. Journal of Magnesium and Alloys, 2019, 7(3): 536−544.

[2] BI Ji, SHEN Jun-qi, HU Sheng-sun, ZHEN Ya-hui, YIN Feng-liang, BU Xian-zheng. Microstructure and mechanical properties of AZ91 Mg alloy fabricated by cold metal transfer additive manufacturing [J]. Materials Letters, 2020, 276: 128185.

[3] JIANG Bin, DONG Zhi-hua, ZHANG Ang, SONG Jiang-feng, PAN Fu-sheng. Recent advances in micro-alloyed wrought magnesium alloys: Theory and design [J]. Transactions of Nonferrous Metals Society of China, 2022, 32(6): 1741−1780.

[4] ZHANG Ye, XU Rui, SUN Wei, WANG Li, TANG Hong-hu. Li extraction from model brine via electrocoagulation: Processing, kinetics, and mechanism [J]. Separation and Purification Technology, 2020, 250: 117234.

[5] PAN Xi-juan, DOU Zhi-he, ZHANG Ting-an, MENG De-liang, FAN Yang-yang. Separation of metal ions and resource utilization of magnesium from saline lake brine by membrane electrolysis [J]. Separation and Purification Technology, 2020, 251: 117316.

[6] ZHANG Ye, XU Rui, WANG Li, SUN Wei. Separation of magnesium from lithium in salt-lake brine through struvite precipitation [J]. Minerals Engineering, 2022, 180: 107468.

[7] LIN S, PAN Y N, DU J L, YANG Y, SU H P, YU J G. Double-edged role of interlayer water on Li^+ extraction from ultrahigh Mg^{2+}/Li^+ ratio brines using Li/Al-LDHs [J]. Journal of Colloid and Interface Science, 2022, 627: 872−879.

[8] ZHANG L C, LI J F, LIU R R, ZHOU Y Q, ZHANG Y Z, JI L M, LI L J. Recovery of lithium from salt lake brine with high Na/Li ratio using solvent extraction [J]. Journal of Molecular Liquids, 2022, 362: 119667.

[9] ZHANG Y, WANG L, SUN W, HU Y H, TANG H H. Membrane technologies for Li^+/Mg^{2+} separation from salt-lake brines and seawater: A comprehensive review [J]. Journal of Industrial and Engineering Chemistry, 2020, 81: 7−23.

[10] ZHAO Z W, SI X F, LIANG X X, LIU X H, HE L H. Electrochemical behavior of Li^+, Mg^{2+}, Na^+ and K^+ in $LiFePO_4/FePO_4$ structures [J]. Transactions of Nonferrous Metals Society of China, 2013, 23(4): 1157−1164.

[11] ZHANG Y, HU Y H, WANG L, SUN W. Systematic review of lithium extraction from salt-lake brines via precipitation approaches [J]. Minerals Engineering, 2019, 139: 105868.

[12] TRAN K T, HAN K S, KIM S J, KIM M J, TRAN T. Recovery of magnesium from Uyuni salar brine as hydrated magnesium carbonate [J]. Hydrometallurgy, 2016, 160: 106−114.

[13] TRAN K T, van LUONG T, AN J W, KANG D J, KIM M J, TRAN T. Recovery of magnesium from Uyuni salar brine as high purity magnesium oxalate [J]. Hydrometallurgy, 2013, 138: 93−99.

[14] GUO H, KUANG G, LI H, PEI W T, WANG H D. Enhanced lithium leaching from lepidolite in continuous tubular reactor using H_2SO_4+H_2SiF_6 as lixiviant [J]. Transactions of Nonferrous Metals Society of China, 2021, 31(7): 2165−2173.

[15] WANG H Y, ZHONG Y, DU B Q, ZHAO Y J, WANG M. Recovery of both magnesium and lithium from high Mg/Li ratio brines using a novel process [J]. Hydrometallurgy, 2018, 175: 102−108.

[16] MOHAPATRA L, PARIDA K. A review on the recent progress, challenges and perspective of layered double hydroxides as promising photocatalysts [J]. Journal of Materials Chemistry A, 2016, 4(28): 10744−10766.

[17] ABINAYA S, KAVITHA H P, PRAKASH M, MUTHUKRISHNARAJ A. Green synthesis of magnesium oxide nanoparticles and its applications: A review [J]. Sustainable Chemistry and Pharmacy, 2021, 19: 100368.

[18] KUTHATI Y, KANKALA R K, LEE C H. Layered double hydroxide nanoparticles for biomedical applications: Current status and recent prospects [J]. Applied Clay Science, 2015, 112: 100−116.

[19] ZHANG Y, HU Y H, SUN N, KHOSO S A, WANG L, SUN W. A novel precipitant for separating lithium from magnesium in high Mg/Li ratio brine [J]. Hydrometallurgy, 2019, 187: 125−133.

[20] HOJAMBERDIEV M, ARIFOV P, TADJIEV K, XU Y H. Processing of refractory materials using various magnesium sources derived from Zinelbulak talc−magnesite [J]. International Journal of Minerals, Metallurgy, and Materials, 2011, 18(1): 105−114.

[21] RAMEZANI A, EMAMI S M, NEMAT S. Effect of waste serpentine on the properties of basic insulating refractories [J]. Ceramics International, 2018, 44(8): 9269−9275.

[22] GU F Q, PENG Z W, ZHANG Y B, TANG H M, YE L, TIAN W G, LIANG G S, LEE J, RAO M J, LI G H, JIANG T. Valorization of ferronickel slag into refractory materials: Effect of sintering temperature [J]. JOM, 2019, 71(3): 1024−1032.

[23] HU J H, REN Q F, YANG D J, MA S W, SHANG J L, DING X T, LUO Z Q. Cross-scale characteristics of backfill material using NMR and fractal theory [J]. Transactions of Nonferrous Metals Society of China, 2020, 30(5): 1347−1363.

[24] XIAO Y, FENG N N, WANG R H, DONG H G, GUO Z W, CUI H, WU H Y, LIU X X, XIE J P. Application of modified sepiolite as reusable adsorbent for Pd(II) sorption from acidic solutions [J]. Transactions of Nonferrous Metals Society of China, 2020, 30(5): 1375−1386.

[25] YUAN L, MA B Y, DU Y L, LI G Q, ZHU Q, YU J K. Characterization and properties of ZrO_2-forsterite composites from zircon and magnesite via reaction sintering [J]. Journal of Ceramic Processing Research, 2017, 18(5): 352−356.

[26] GU F Q, PENG Z W, ZHANG Y B, TANG H M, YE L, TIAN W G, LIANG G S, RAO M J, LI G H, JIANG T. Facile route for preparing refractory materials from ferronickel slag with addition of magnesia [J]. ACS Sustainable Chemistry & Engineering, 2018, 6(4): 4880−4889.

[27] PAGONA E, KALAITZIDOU K, ZOUBOULIS A, MITRAKAS M. Effects of additives on the physical properties of magnesite ore mining by-products for the production of refractories [J]. Minerals Engineering, 2021, 174: 107247.

[28] TANG H M, PENG Z W, GU F Q, YE L, HWANG J Y, RAO M J, LI G H, JIANG T. Alumina-enhanced valorization of ferronickel slag into refractory materials under microwave irradiation [J]. Ceramics International, 2020, 46(5): 6828−6837.

[29] LI J, WANG Q, LIU J H, LI P. Synthesis process of forsterite refractory by iron ore tailings [J]. Journal of Environmental Sciences, 2009, 21(Suppl.): 92−95.

[30] BERNARD E, LOTHENBACH B, CHLIQUE C, WYRZYKOWSKI M, DAUZERES A, POCHARD I, CAU-DIT-COUMES C. Characterization of magnesium silicate hydrate (M−S−H) [J]. Cement and Concrete Research, 2019, 116: 309−330.

[31] von HOESSLE F, MOHAMED M, FARID R,

HAMMOUDA R M, KÜHN F E, BASSIONI G. Interfacial phenomena of magnesium hydroxide micro phases [J]. Ain Shams Engineering Journal, 2021, 12(3): 3133−3140.

[32] REN H, LIU J, MA S. Introduction to inorganic chemistry of energetic materials [M]. Beijing: Beijing Institute of Technology Press, 2020. (in Chinese)

[33] XU C H, WANG F, LIU D J, CHEN W. Effect of additive EDTA on crystallization process of magnesium hydroxide precipitation [J]. Chinese Journal of Chemical Engineering, 2010, 18(5): 761−766.

[34] REN X M, MA B Y, FU G F, QIAN F, LIU G Q, YU J K, LI Y W. Facile synthesis of $MgO-Mg_2SiO_4$ composite ceramics with high strength and low thermal conductivity [J]. Ceramics International, 2021, 47(14): 19959−19969.

[35] JU J T, TANG C M, JI G H, XING X D, ZHAO G Q, JIANG X T, LU F L. Effect of $BaSO_4$ on phase composition and sintering process of iron ore fines [J]. Journal of Iron and Steel Research International, 2022, 29(3): 408−417.

[36] YANG J, XU L H, WU H Q, JIN J. Preparation and properties of porous ceramics from spodumene flotation tailings by low-temperature sintering [J]. Transactions of Nonferrous Metals Society of China, 2021, 31(9): 2797−2811.

[37] WANG J A, NOVARO O, BOKHIMI X, LÓPEZ T, GÓMEZ R, NAVARRETE J, LLANOS M E, LÓPEZ-SALINAS E. Characterizations of the thermal decomposition of brucite prepared by sol−gel technique for synthesis of nanocrystalline MgO [J]. Materials Letters, 1998, 35(5): 317−323.

[38] L'VOV B V, NOVICHIKHIN A V, DYAKOV A O. Mechanism of thermal decomposition of magnesium hydroxide [J]. Thermochimica Acta, 1998, 315: 135−143.

[39] YANG W, ZHU Z J, SHI J J, ZHAO B, CHEN Z Q, WU Y C. Characterizations of the thermal decomposition of nano-magnesium hydroxide by positron annihilation lifetime spectroscopy [J]. Powder Technology, 2017, 311: 206−212.

[40] ACAR I. Sintering properties of olivine and its utilization potential as a refractory raw material: Mineralogical and microstructural investigations [J]. Ceramics International. 2020, 46(18A): 28025−28034.

[41] LAFAY R, MONTES-HERNANDEZ G, JANOTS E, MUNOZ M, AUZENDE A L, GEHIN A, CHIRIAC R, PROUX O. Experimental investigation of As, Sb and Cs behavior during olivine serpentinization in hydrothermal alkaline systems [J]. Geochimica et Cosmochimica Acta, 2016, 179: 177−202.

[42] NEMAT S, RAMEZANI A, EMAMI S M. Possible use of waste serpentine from Abdasht chromite mines into the refractory and ceramic industries [J]. Ceramics International, 2016, 42(16): 18479−18483.

[43] DLUGOGORSKI B Z, BALUCAN R D. Dehydroxylation of serpentine minerals: Implications for mineral carbonation [J]. Renewable and Sustainable Energy Reviews, 2014, 31: 353−367.

[44] MICHEL R, AMMAR M R, POIRIER J, SIMON P. Phase transformation characterization of olivine subjected to high temperature in air [J]. Ceramics International, 2013, 39(5): 5287−5294.

采用沉淀−煅烧法回收盐湖卤水中镁资源制备镁橄榄石耐火材料

张 烨[1,2]，胡岳华[2]，王 丽[2]，孙 伟[2]

1. 华东理工大学 化工学院 国家盐湖资源综合利用工程技术研究中心，上海 200237；
2. 中南大学 资源加工与生物工程学院 战略含钙矿物资源清洁高效利用湖南省重点实验室，长沙 410083

摘 要：通过沉淀−煅烧法研究盐湖锂镁分离和镁资源制备高附加值的镁橄榄石耐火材料。采用 Na_2SiO_3 和 NaOH 组合沉淀剂将盐湖卤水中的锂、镁离子沉淀分离，获得不同 MgO/SiO_2 摩尔比的镁沉淀物。镁沉淀物主要由无定形硅酸镁和氢氧化镁堆积而成，在 1400 ℃条件下的质量残留率均在 62%以上。高温烧结实验表明，在 Mg/Na_2SiO_3/NaOH 的摩尔比为 1:0.6:0.8、烧结温度为 1350 ℃、时间为 210 min 的条件下，镁沉淀物可制备成性能优良的耐火材料，其耐火度在 1800 ℃以上，抗压强度为 190.73 MPa，体积密度为 2.53 g/cm^3，显气孔率为 5.94%。所制备的耐火材料主要为镁橄榄石相，含有少量的顽火辉石相。

关键词：盐湖卤水；组合沉淀剂；锂镁沉淀分离；镁沉淀物；镁橄榄石耐火材料

(Edited by Wei-ping CHEN)